



JOURNAL ON COMMUNICATIONS

ISSN:1000-436X

Scopus®

REGISTERED

www.jocs.review

Robust Stabilization of an Inverted Pendulum with a Reaction Wheel with Polytopic Uncertainties via LMIs

Jonatas Bernardino dos Santos[1], Luciano Diz da Silva[1], Rodrigo Henrique Silva de Souza[1], Fernando Sabino Fonteque Ribeiro[2], Ricardo Breganon[1*] and Uiliam Nelson Lendzion Tomaz Alves[1]

[1]*Federal Institute of Education, Science and Technology of Paraná (IFPR), Jacarezinho, Paraná, Brazil.*
[2]*State University of Maringá (UEM), Maringá, Paraná, Brazil.*

*Corresponding Author: Ricardo Breganon

Abstract: *This paper presents the design and experimental validation of a robust state-feedback controller for a Reaction Wheel Inverted Pendulum (RWIP) subject to three parametric uncertainties: the reaction wheel's moment of inertia, the reaction wheel's mass, and the counterweight's mass. In this way, the RWIP serves as a case study for a didactic tool for teaching robust control. The controller is synthesized via Linear Matrix Inequalities (LMIs), ensuring a minimum decay rate and constraining the norm of the feedback gain to limit actuator effort. The dynamic model combines the mechanical dynamics of the pendulum and the reaction wheel, obtained via Lagrange's equations, with the electromechanical model of the direct current motor, neglecting the armature inductance. This model is then linearized and written as a polytopic uncertain system with eight vertices. We solved the LMIs in MATLAB using the YALMIP parser and the SeDuMi solver. The controller was evaluated in simulation and implemented in a physical prototype, with the system subjected to rectangular pulse disturbances in both scenarios. Experimental results, assessed through the IAE, ISE, ITAE, and ITSE indices, confirm the robustness of the proposed strategy, which stabilizes the system with a convergence compatible with the imposed decay rate, while operating within the actuator saturation limits.*

Keywords: **Robust control; Reaction wheel inverted pendulum; Linear matrix inequalities; Experimental application; Decay rate.**

1. Introduction

The inverted pendulum is one of the most widely used benchmark systems in teaching and research on dynamic system control. Its nonlinear behavior and unstable equilibrium point make it a well-established didactic platform for applying and comparing several control strategies [1], and it is widely used in laboratory experimental setups [2]. Beyond the educational context, dynamics analogous to those of the inverted pendulum appear in wind turbines [3], biped robots [4], and the human body [5], reinforcing the practical relevance of studying these control techniques.

Different approaches have been investigated for this system, including PID and Fuzzy controllers [6], the Linear Quadratic Regulator (LQR) [7] and robust methods such as H_2 [8] and H_∞ [9].

The reaction wheel (RW) is a high-precision actuator, commonly used in satellite attitude control [10]. It has also been explored as a stabilization mechanism in biped robots by controlling the Zero-Moment-Point (ZMP) [4]. Combining an inverted pendulum with a reaction wheel creates a system with greater dynamic complexity, broadening the possibilities for investigating advanced control strategies.

In controller design, the decay rate of the state variables determines the system's convergence speed, but increasing it implies a larger feedback-gain norm and, consequently, greater actuator effort. The trade-off between these two requirements, together with the treatment of parametric uncertainties, motivates the use of robust controllers synthesized via Linear Matrix Inequalities (LMIs) [11-14].

This work extends the controller proposed in [15] by explicitly incorporating three parametric uncertainties in the synthesis and experimental validation. The same prototype was also used in [16], where pole-placement and LQR state-feedback controllers, combined with an energy-based swing-up strategy, were designed and compared experimentally, without considering parametric uncertainties. The main contribution is the design of a robust state-feedback controller via LMIs, with a guaranteed minimum decay rate and a bounded gain norm, implemented and validated on a Reaction Wheel Inverted Pendulum (RWIP) prototype. In addition to the robust control results, the prototype used demonstrates potential as a didactic tool in courses of control systems, robust control, and nonlinear systems, in line with the pedagogical approach discussed in [2]; this work therefore serves as a case study of the use of a prototype in the test of control strategies.

The remainder of the paper is structured as follows: Section 2 presents the dynamic model and the RWIP prototype; Section 3 details the theorems used in the controller design; and Sections 4 and 5 present simulation and experimental results and the conclusions, respectively.

2. Reaction Wheel Inverted Pendulum (RWIP)

2.1. Dynamic Model

Figure 1 presents a schematic diagram of the RWIP. The indicated parameters are: $\sigma(t)$ - angular position of the pendulum; $\phi(t)$ - angular position of the reaction wheel (RW); M_{tr} - set of masses composed of: M_a - mass of the coupling of the RW to the motor, M_r - mass of the RW and M_m - mass of the motor; M_{h1} and M_{h2} - mass of each half of the rod to which the RW and the counterweight are fixed, respectively; L_{ch1} and L_{ch2} - distances from the centre of mass M_{h1} and M_{h2} to the axis of rotation; M_c - mass of the counterweight; L_{h1} and L_{h2} - distance from the axis of rotation to the end of the rod; L_{h3} and L_{h4} - distance from the axis of rotation to the points where M_{tr} and M_c are fixed, respectively; I_r - inertia of the RW; and I_h - inertia of the rod.

For modeling the RWIP, it is necessary to consider the dynamics of the direct current (DC) motor together with those of the pendulum. Neglecting the motor's inductance, the torque on the output shaft of the gear motor can be computed as [15], [17]:

$$\tau(t) = \frac{\eta K_t V(t)}{R_a} - \frac{\eta^2 K_t K_v \dot{\phi}(t)}{R_a} - A_m \dot{\phi}(t), \tag{1}$$

where η represents the gear reduction of the motor, K_t the torque constant, K_v the back-electromotive force constant, A_m the viscous friction coefficient of the DC motor, $\dot{\phi}(t)$ the angular velocity of the RW, $V(t)$ the voltage applied to the DC motor and, finally, R_a the armature resistance.

Using the Lagrange equation of motion, the nonlinear dynamic model of the RWIP is derived [17]:

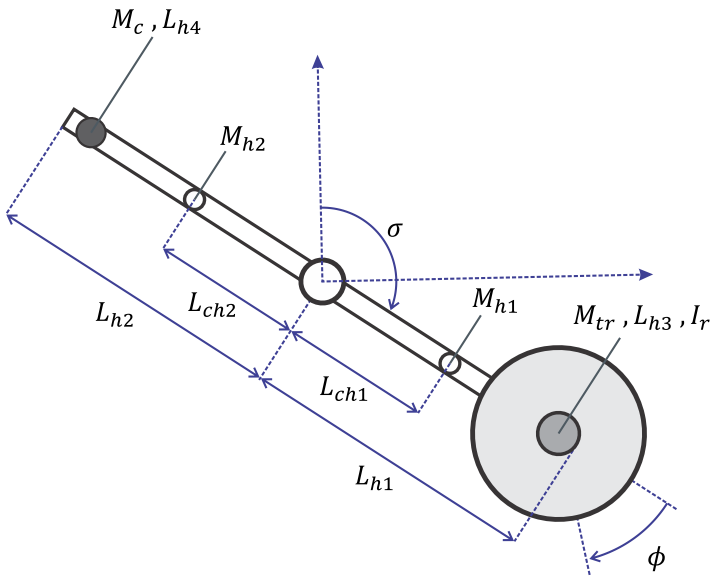


Figure 1. Schematic diagram of the RWIP.
Source: [15], (2026).

$$\ddot{\sigma}(t) = \frac{1}{I_p I_r - I_r^2}\left[-I_r\tau(t) + I_r\overline{M}_1 g\sin\left(\sigma(t)\right) - I_r\overline{M}_2 g\sin(\sigma(t))\right],$$
$$\ddot{\phi}(t) = \frac{1}{I_p I_r - I_r^2}\left[I_p\tau(t) + I_r\overline{M}_2 g\sin\left(\sigma(t)\right) - I_r\overline{M}_1 g\sin(\sigma(t))\right], \quad (2)$$

where

$$I_p = \frac{1}{3}M_{h1}L_{h1}^2 + \frac{1}{3}M_{h2}L_{h2}^2 + M_{tr}L_{h3}^2 + M_c L_{h4}^2 + I_h,$$
$$\overline{M}_1 = M_{h1}L_{ch1} + M_{tr}L_{h3},$$
$$\overline{M}_2 = M_{h2}L_{ch2} + M_c L_{h4}.$$

Combining (2) and (1), the nonlinear dynamic model of the prototype is obtained. Linearizing the equations at the operating point where the pendulum is perpendicular to the ground and the reaction wheel is positioned at the upper part yields

$$\ddot{\sigma}(t) = \frac{I_r\overline{M}_1 g\sigma(t)}{S_i} - \frac{I_r\overline{M}_2 g\sigma(t)}{S_i} - \frac{I_r\eta K_t V(t)}{S_i R_a} + \frac{I_r\eta^2 K_t K_v\dot{\phi}(t)}{S_i R_a} + \frac{I_r A_m\dot{\phi}(t)}{S_i},$$
$$\ddot{\phi}(t) = \frac{I_r\overline{M}_2 g\sigma(t)}{S_i} - \frac{I_r\overline{M}_1 g\sigma(t)}{S_i} + \frac{I_p\eta K_t V(t)}{S_i R_a} - \frac{I_p\eta^2 K_t K_v\dot{\phi}(t)}{S_i R_a} - \frac{I_p A_m\dot{\phi}(t)}{S_i}, \quad (3)$$

where $S_i = I_p I_r - I_r^2$. Further details of the methodology used in the modeling of the RWIP are presented in [17]. The dynamics (3) can be represented in state space as

$$\dot{x}(t) = Ax(t) + Bu(t), \quad (4)$$

$$A = \begin{bmatrix} 0 & 1 & 0 \\ \dfrac{I_r\overline{M}_1 g - I_r\overline{M}_2 g}{S_i} & 0 & \dfrac{I_r\eta^2 K_t K_v + I_r A_m R_a}{S_i R_a} \\ \dfrac{I_r\overline{M}_2 g - I_r\overline{M}_1 g}{S_i} & 0 & -\dfrac{I_p\eta^2 K_t K_v + I_p A_m R_a}{S_i R_a} \end{bmatrix}, \quad B = \begin{bmatrix} 0 \\ -\dfrac{I_r\eta K_t}{S_i R_a} \\ \dfrac{I_p\eta K_t}{S_i R_a} \end{bmatrix}, \quad (5)$$

in which $x(t) = [\sigma(t) \quad \dot{\sigma}(t) \quad \dot{\phi}(t)]^T$ is the state vector and $u(t) = V(t)$.

2.2. Prototype

Figure 2 shows the RWIP prototype used in the tests, with its main components labeled [15], [16]. ❶ - Reaction Wheel (RW) fixed to the direct current (DC) motor; together, they generate the torque that changes the angular position of the pendulum; ❷ - CHP-36GP-555-ABHL 12 V, 1100 rpm DC motor that rotates the RW; ❸ - encoder with 350 pulses per revolution coupled to the DC motor, responsible for determining its angular position; ❹ - metallic rod that connects the RW assembly to the counterweight; ❺ - counterweight; ❻ - slip ring with a central hole that allows the electrical connection of ❷ and ❸ without twisting the cables; ❼ - LPD3806-600BM-G5-24C rotary encoder responsible for determining the angular position of the pendulum; ❽ - HW-039 H-bridge, 43 A, 5-36 V, responsible for controlling the direction and speed of the DC motor; ❾ - ESP32 microcontroller responsible for reading encoder data and driving the motor; ❿ - MPC-3003 voltage source that supplies power to the components of the prototype; ⓫ - emergency button; ⓬ - computer that controls the prototype using MATLAB® Simulink software, with an AMD Phenom™ II X2 B57 3.20 GHz processor and 12 GB of RAM.

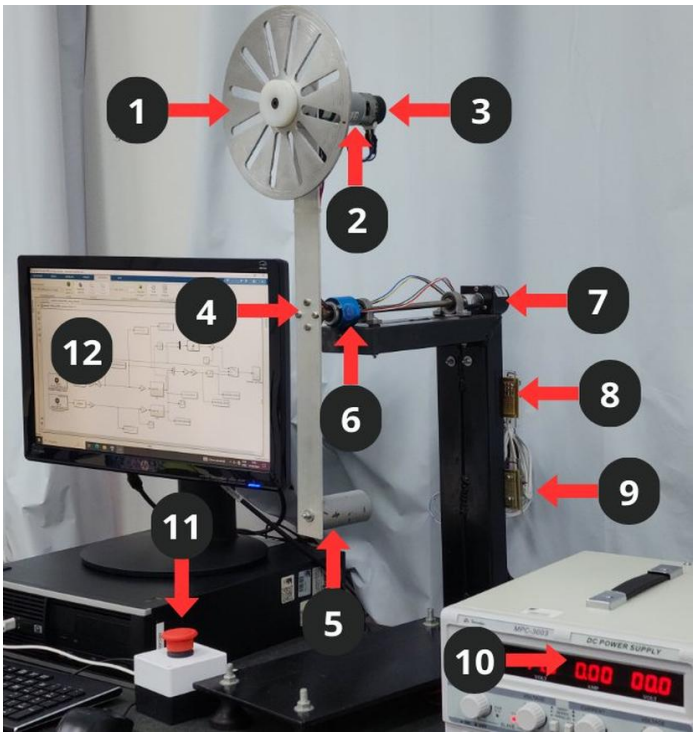


Figure 2. Prototype of the Reaction Wheel Inverted Pendulum.
Source: Adapted from [15], (2026).

Tables 1 and 2 present the physical parameters of the prototype and the DC motor used to design the controller. These parameters were also used in the simulations, whose results are compared with the experiments on the prototype in Section 4. In this work it is considered that the inertia and the mass of the RW, as well as the mass of the counterweight, are uncertain parameters such that $I_{r1} \leq I_r \leq I_{r2}$; $M_{r1} \leq M_r \leq M_{r2}$ and $M_{c1} \leq M_c \leq M_{c2}$.

Given the uncertain parameters, the uncertain system (4) can be represented by [11]

$$\dot{x}(t) = A(\alpha)x(t) + B(\alpha)u(t), \tag{6}$$

$$A(\alpha) = \sum_{i=1}^{N} \alpha_i A_i, \quad B(\alpha) = \sum_{i=1}^{N} \alpha_i B_i, \quad \sum_{i=1}^{N} \alpha_i = 1, \ \alpha \geq 0,$$

where $A_i \in \mathbb{R}^{n_x \times n_x}$ and $B_i \in \mathbb{R}^{n_x \times n_u}$ are known matrices, and $N = 2^s$, s is the number of parameters with uncertain values. For the case under study, $n_x = 3$, $n_u = 1$ and $N = 8$.

Table 1. Physical parameters of the RWIP.

Symbol	Description [unit]	Values
L	Rod length [m]	0.5
L_{h1} and L_{h2}	Rod length with respect to the pivot [m]	0.25
L_{ch1} and L_{ch2}	Distance from the pivot to the center of mass of the rod [m]	0.125
L_{h3}	Distance from the pivot to the center of mass of the wheel [m]	0.2278
L_{h4}	Distance from the pivot to the center of mass of the counterweight [m]	0.2272
M_{c1}	Mass of counterweight 1 [kg]	0.580
M_{c2}	Mass of counterweight 2 [kg]	0.645
M_h	Rod mass [kg]	0.171
M_{h1} and M_{h2}	Mass of half of the rod [kg]	0.0855
M_m	Motor mass [kg]	0.390
M_{r1}	Mass of wheel 1 [kg]	0.22582
M_{r2}	Mass of wheel 2 [kg]	0.29278
M_a	Mass of the wheel coupling [kg]	0.08692
I_{r1}	Moment of inertia of wheel 1 [kg·m²]	1.148×10^{-3}
I_{r2}	Moment of inertia of wheel 2 [kg·m²]	1.653×10^{-3}
I_h	Moment of inertia of the rod [kg·m²]	8.1049×10^{-7}
g	Acceleration of gravity [m/s²]	9.81

Table 2. Parameters of the DC motor.

Symbol	Description [unit]	Values
A_m	Friction coefficient of the motor [N·m·s/rad]	0.0014
I_{a0}	No-load armature current [A]	0.28
$\dot{\varphi}$	No-load speed [rpm]	1100
τ_e	Rated electrical torque [N·m]	0.1882
$\dot{\phi}$	Rated speed [rpm]	880
I_a	Rated armature current [A]	≤ 2.0
τ_{eb}	Locked-rotor torque [kgf·cm]	≥ 7.0
I_{ab}	Locked-rotor armature current [A]	≤ 9.5
R_a	Armature resistance [Ω]	1.6632
K_t	Torque constant [N·m/A]	0.01811
K_v	Back-EMF constant [V/(rad/s)]	0.01811
η	Gear reduction of the motor	5.2

Using the values of Tables 1 and 2, from the matrices in (5), the following vertices are obtained

$$A_1 = \begin{bmatrix} 0 & 1 & 0 \\ 4.0139 & 0 & 0.0977 \\ -4.0139 & 0 & -5.9549 \end{bmatrix}, A_2 = \begin{bmatrix} 0 & 1 & 0 \\ 4.0435 & 0 & 0.0984 \\ -4.0435 & 0 & -4.1675 \end{bmatrix},$$

$$A_3 = \begin{bmatrix} 0 & 1 & 0 \\ 5.8899 & 0 & 0.0930 \\ -5.8899 & 0 & -5.9502 \end{bmatrix}, A_4 = \begin{bmatrix} 0 & 1 & 0 \\ 5.9313 & 0 & 0.0937 \\ -5.9313 & 0 & -4.1628 \end{bmatrix},$$

$$A_5 = \begin{bmatrix} 0 & 1 & 0 \\ 1.8368 & 0 & 0.0932 \\ -1.8368 & 0 & -5.9504 \end{bmatrix}, A_6 = \begin{bmatrix} 0 & 1 & 0 \\ 1.8497 & 0 & 0.0938 \\ -1.8497 & 0 & -4.1629 \end{bmatrix}, \quad (7)$$

$$A_7 = \begin{bmatrix} 0 & 1 & 0 \\ 3.7302 & 0 & 0.0889 \\ -3.7302 & 0 & -5.9461 \end{bmatrix}, A_8 = \begin{bmatrix} 0 & 1 & 0 \\ 3.7553 & 0 & 0.0895 \\ -3.7553 & 0 & -4.1586 \end{bmatrix},$$

$$B_1 = \begin{bmatrix} 0 \\ -0.8219 \\ 50.1006 \end{bmatrix}, B_2 = \begin{bmatrix} 0 \\ -0.8280 \\ 35.0625 \end{bmatrix}, B_3 = \begin{bmatrix} 0 \\ -0.7824 \\ 50.0611 \end{bmatrix}, B_4 = \begin{bmatrix} 0 \\ -0.7879 \\ 35.0225 \end{bmatrix}, \quad (8)$$

$$B_5 = \begin{bmatrix} 0 \\ -0.7840 \\ 50.0627 \end{bmatrix}, B_6 = \begin{bmatrix} 0 \\ -0.7895 \\ 35.0240 \end{bmatrix}, B_7 = \begin{bmatrix} 0 \\ -0.7480 \\ 50.0267 \end{bmatrix}, B_8 = \begin{bmatrix} 0 \\ -0.7530 \\ 34.9875 \end{bmatrix}.$$

3. Robust Controller Design with Decay Rate and Controller Gain Norm Constraints

The decay rate of a system is directly related to the convergence speed of the system's state variables; therefore, it is an important performance criterion for controller design. The decay rate is defined as the largest positive constant γ such that

$$\lim_{t\to\infty} e^{\gamma t}\|x(t)\| = 0$$

is valid for all the trajectories $x(t)$, $t > 0$ [11].

Using the quadratic Lyapunov function $V(x(t)) = x(t)^T P x(t)$, $P = P^T > 0 \in \mathbb{R}^{n_x \times n_x}$, it is possible to determine a lower bound on the decay rate of the controlled system using the constraint $\dot{V}(x(t)) \leq -2\gamma V(x(t))$ [11].

Consider the control law for state feedback given by

$$u(t) = -Kx(t), \quad (9)$$

where $K \in \mathbb{R}^{n_u \times n_x}$ is a gain matrix.

Theorem 1 [11]: Consider system (6) in closed loop and with control law (9). For a given $\gamma > 0$, if there exist a matrix $M \in \mathbb{R}^{n_u \times n_x}$ and a symmetric and positive definite matrix $X \in \mathbb{R}^{n_x \times n_x}$ such that

$$XA_i^T - M^T B_i^T + A_i X - B_i M + 2\gamma X < 0, \quad (10)$$

for all $i = 1$ up to N, then the control law (9), with $K = MX^{-1}$, makes system (6) asymptotically stable and with a decay rate greater than or equal to γ.

Proof: See [11].

In systems controlled by state feedback, the norm of the gain matrix K affects the performance of the closed-loop system, and a large value may hinder implementation due to the actuator's required effort. A workaround for this difficulty is to limit the norm of the feedback gain in exchange for a slower response [15]. This is possible using the conditions given in Theorem 2.

Theorem 2 [12]: Given a constant $\mu_0 > 0$ and a variable $\beta > 0$, the norm of $K = MX^{-1}$ in (9) satisfies the constraint $K^T K < \frac{\beta}{\mu_0} I_{n_x}$ if, together with (10), the following are satisfied

$$\begin{bmatrix} X & M^T \\ M & \beta I_{n_u} \end{bmatrix} > 0, \quad X > \mu_0 I_{n_x}, \tag{11}$$

where I_{n_u} and I_{n_x} are the identity matrices with order equal to the number of inputs and of state variables, respectively.

Proof: See [12].

4. Results and Discussions

The gain matrix K was obtained using the SeDuMi solver [18], the YALMIP parser [19], and the LMIs (10) and (11) proposed in Theorems 1 and 2 in the MATLAB® environment, considering matrices (7) and (8). The parameters used were $\mu_0 = 2$ and $\gamma = 0.5515$, both obtained empirically. Solving the LMIs to minimize β, $\beta = 13527.3818$ was obtained and

$$K = [-58.0502 \quad -31.9584 \quad -0.4604]. \tag{12}$$

With the gain K in (12), all eigenvalues of the closed-loop matrices $A_i - B_i K$, for $i = 1, \ldots, 8$, have real parts smaller than or equal to -0.595, that is, smaller than $-\gamma = -0.5515$, which confirms the minimum decay rate guaranteed by Theorem 1 at all vertices of the polytope. To run the simulations and the prototype experiment, we used the disturbance signal $d(t)$ in (13) acting on the direct-current motor coupled to the reaction wheel, generating an angular variation in the RWIP. The disturbance signal is described as

$$d(t) = \begin{cases} 0\ \text{V}, & t < 5\ \text{s or } 9\ \text{s} \le t < 20\ \text{s or } t \ge 24\ \text{s} \\ 3\ \text{V}, & 5\ \text{s} \le t < 7\ \text{s or } 20\ \text{s} \le t < 22\ \text{s} \\ -3\ \text{V}, & 7\ \text{s} \le t < 9\ \text{s or } 22\ \text{s} \le t < 24\ \text{s}. \end{cases} \tag{13}$$

Using matrix K in (12), we implemented the controller on the physical prototype and in simulations, with a sampling period of 1 ms. A frequency of 490 Hz was used in the PWM sent to the H-bridge. A saturator was included at the controller's output to limit the control action to $\pm 12\,V$, guaranteeing the actuator operating limit. The simulation used the nonlinear RWIP model (1)–(2). Each configuration in Figures 3 to 6 combines one value of each uncertain parameter from Table 1: M_{c1} or M_{c2} (counterweight 1 or 2), and M_{r1} with I_{r1} (wheel 1) or M_{r2} with I_{r2} (wheel 2). The results of the simulation and of the implementation on the prototype for the configurations (M_{c2}, M_{r1} and I_{r1}) and (M_{c2}, M_{r2} and I_{r2}) are presented in Figures 3 and 4, respectively, and those for the configurations (M_{c1}, M_{r1} and I_{r1}) and (M_{c1}, M_{r2} and I_{r2}) in Figures 5 and 6, respectively. The implementation results on the RWIP prototype are available at https://youtu.be/Kgf9XtNu14g.

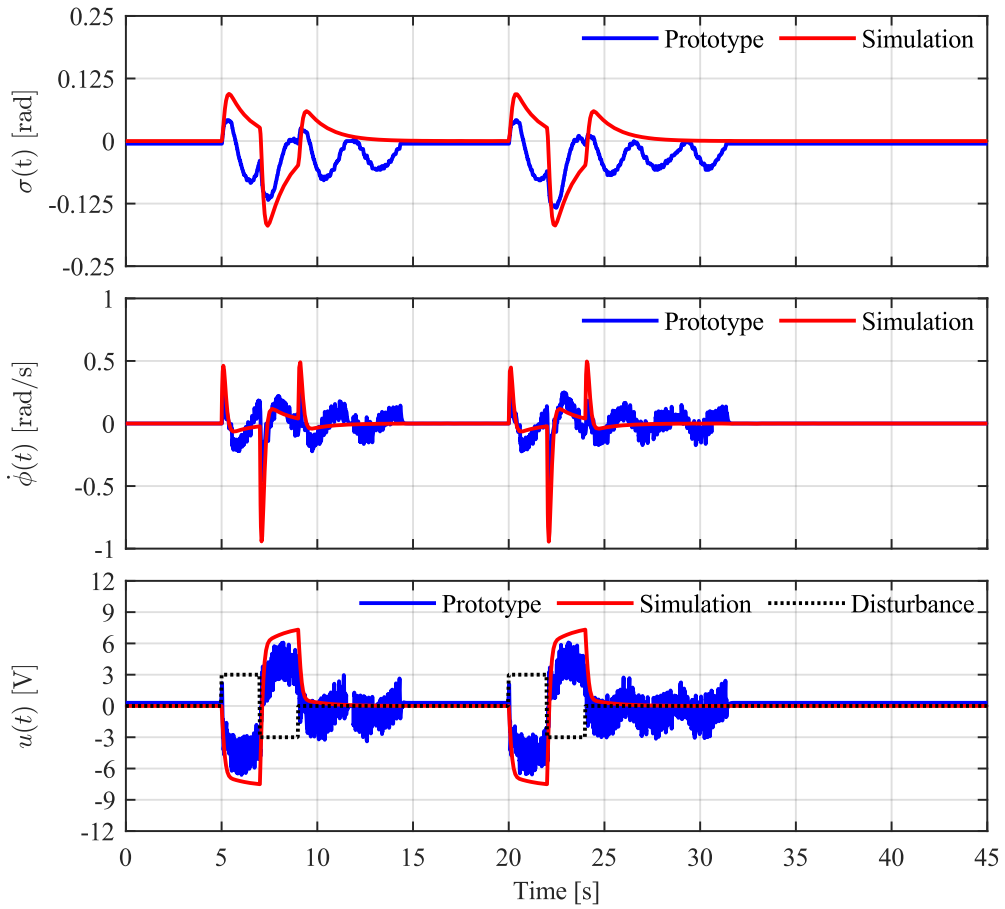


Figure 3. Results of simulation and of implementation on the RWIP prototype in the configuration M_{c2}, M_{r1} and I_{r1}.
Source: Authors, (2026).

From the data in Figures 3 to 6, the controller kept the RWIP near the equilibrium point during disturbances while stabilizing the angular position $\sigma(t)$ and the reaction-wheel angular velocity $\dot{\phi}(t)$. The absence of saturation in the control signal ($|u(t)| \leq 12$ V) is consistent with the effect of the constraint on the norm of the gain of the controller proposed in Theorem 2.

In the experiments using the M_{r2} and I_{r2} configuration, the system required an average of 7 seconds longer to reach steady state after the second disturbance than with the M_{r1} and I_{r1} configuration.

Table 3 presents the performance metrics for the experiments and simulations. Considering the error as the difference between the angular position of the RWIP with respect to its equilibrium point, therefore $e(t) = \sigma(t) - 0$. The analyzed metrics, where $T = 45$ s, are given by [20]

$$\text{IAE} = \int_0^T |e(t)|\, dt, \quad \text{ISE} = \int_0^T e^2(t) dt, \quad \text{ITAE} = \int_0^T t\,|e(t)| dt, \quad \text{ITSE} = \int_0^T t\, e^2(t) dt.$$

It is observed that the configurations with M_{r2} and I_{r2} present lower indices on the prototype, indicating that a greater mass and inertia of the RW reduce the angular deviations of the RWIP. In the simulations, however, M_{r1} and I_{r1} show better metrics. This trend is consistent with the linearized model: for M_{c1}, the configuration with M_{r1} and I_{r1} has a smaller gravitational term (a_{21}=4.0139 in A_1, versus 5.9313 in A_4) and a larger input gain in magnitude ($|b_2| = 0.8219$ versus 0.7879), so the nominal system is less unstable and

easier to stabilize. The consistent advantage of wheel 2 observed on the prototype, as well as the differences between the experimental and simulated indices, can be attributed to effects not included in the model, such as Coulomb (static) friction, mechanical backlash, and unbalance, whose influence is possibly attenuated by the greater mass and inertia of wheel 2.

Table 3. Performance metrics of the experiment on the prototype and the simulations in different system configurations.

Configuration	IAE	ISE	ITAE	ITSE
Experiment (M_{c2}, M_{r1}, I_{r1})	0.9562	0.05304	17.9536	0.9070
Simulation (M_{c2}, M_{r1}, I_{r1})	0.8170	0.06925	12.5785	1.0392
Experiment (M_{c2}, M_{r2}, I_{r2})	0.4194	0.01091	8.3513	0.1836
Simulation (M_{c2}, M_{r2}, I_{r2})	0.7242	0.06045	11.1158	0.9170
Experiment (M_{c1}, M_{r1}, I_{r1})	0.6314	0.02547	11.6340	0.3854
Simulation (M_{c1}, M_{r1}, I_{r1})	0.5472	0.04701	8.2817	0.7045
Experiment (M_{c1}, M_{r2}, I_{r2})	0.3419	0.00759	6.9574	0.1317
Simulation (M_{c1}, M_{r2}, I_{r2})	0.5629	0.04657	8.5776	0.7048

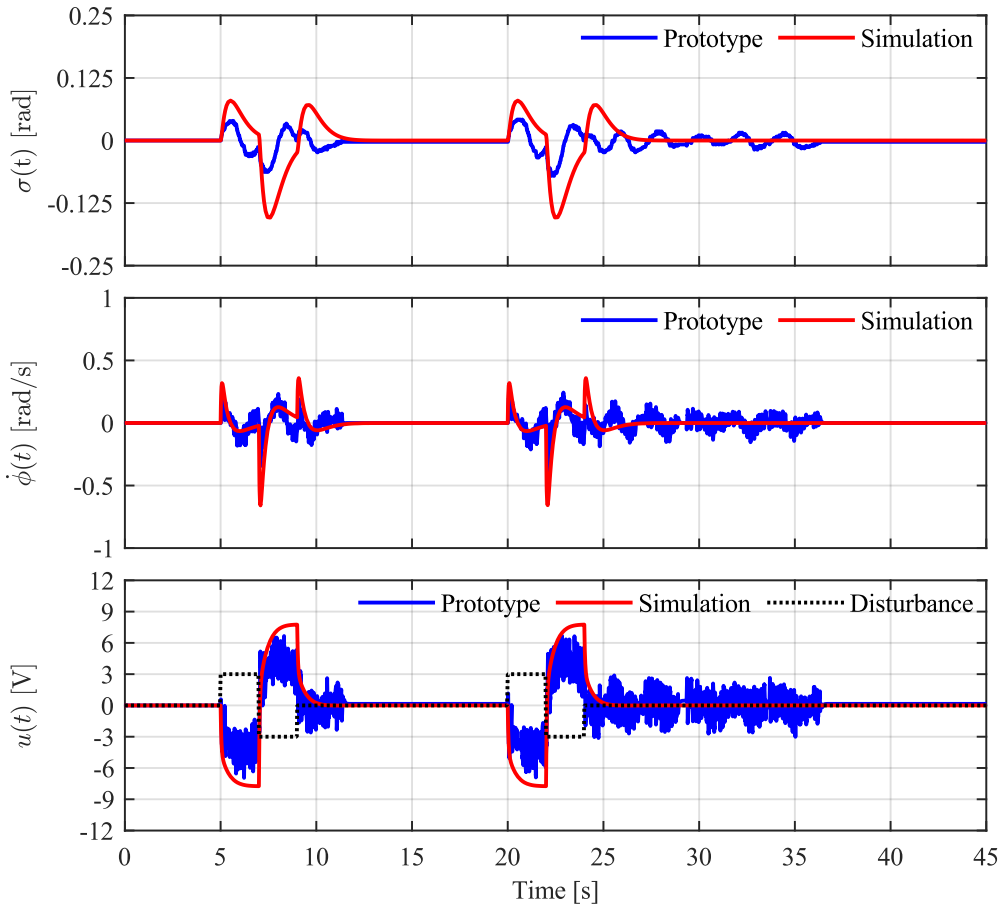


Figure 4. Results of simulation and of implementation on the RWIP prototype in the configuration M_{c2}, M_{r2} and I_{r2}.
Source: Authors, (2026).

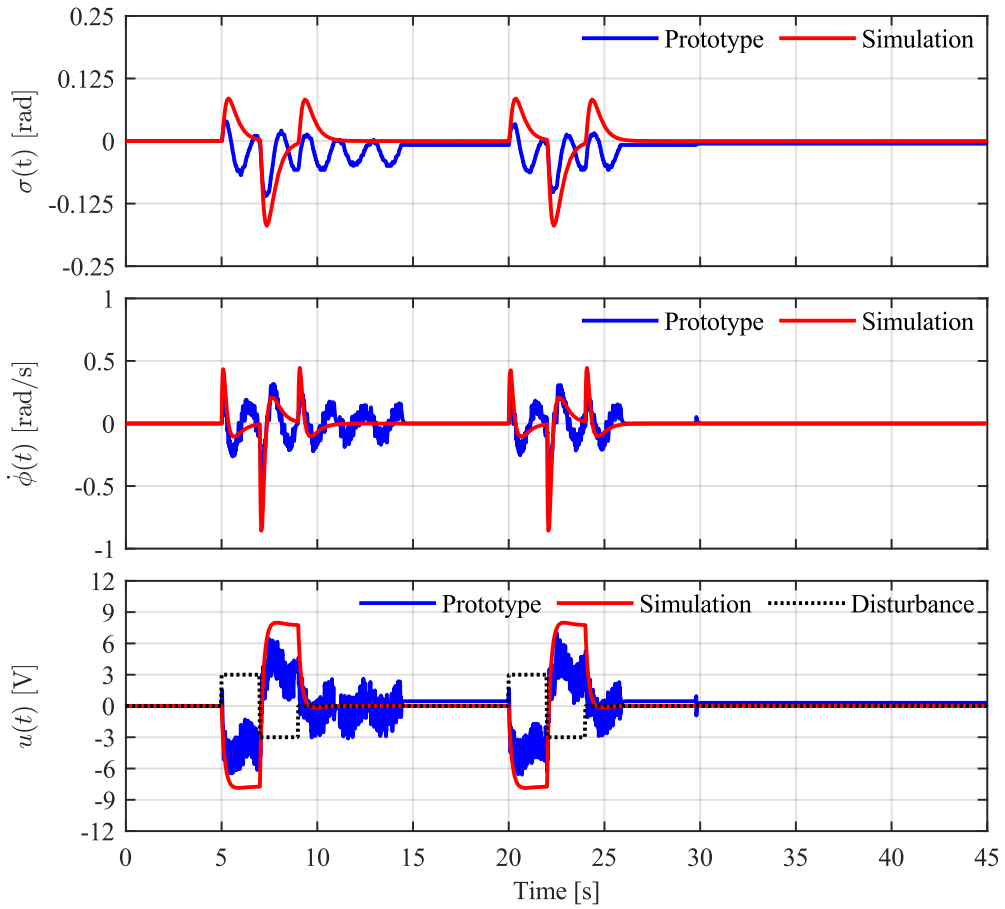


Figure 5. Results of simulation and of implementation on the RWIP prototype in the configuration M_{c1}, M_{r1} and I_{r1}.
Source: Authors, (2026).

Quantitatively, on the prototype, replacing wheel 1 with wheel 2 reduced the IAE by approximately 56% with counterweight 2 (from 0.9562 to 0.4194) and by 46% with counterweight 1 (from 0.6314 to 0.3419), with even larger reductions in the ISE (79% and 70%, respectively). For the same wheel, counterweight 1 led to lower indices than counterweight 2, both in the experiments and in the simulations. For wheel 2, all experimental indices are lower than the simulated ones, whereas for wheel 1 the experimental IAE and ITAE are higher than the simulated values and the experimental ISE and ITSE are lower. Since the quadratic indices penalize large errors more heavily, this indicates that, with wheel 1, the prototype presents smaller angular peaks than predicted, but small residual deviations that persist for longer, a behavior compatible with the static friction and backlash mentioned above.

5. Conclusions

In this work, we proposed a robust controller with a decay-rate and gain-norm constraints, implemented in a prototype Reaction Wheel Inverted Pendulum (RWIP). The results confirm that the controller stabilizes the system and resists disturbances even in the presence of parametric variations. The prototype also demonstrated potential as a didactic case study for teaching robust control via LMIs, allowing different physical configurations to be tested and the effects of parametric uncertainties on controller performance to be observed experimentally. Future work will integrate the swing-up strategy validated on this

prototype in [16] with the proposed robust controller and compare its performance with other control approaches, such as Fuzzy and PID.

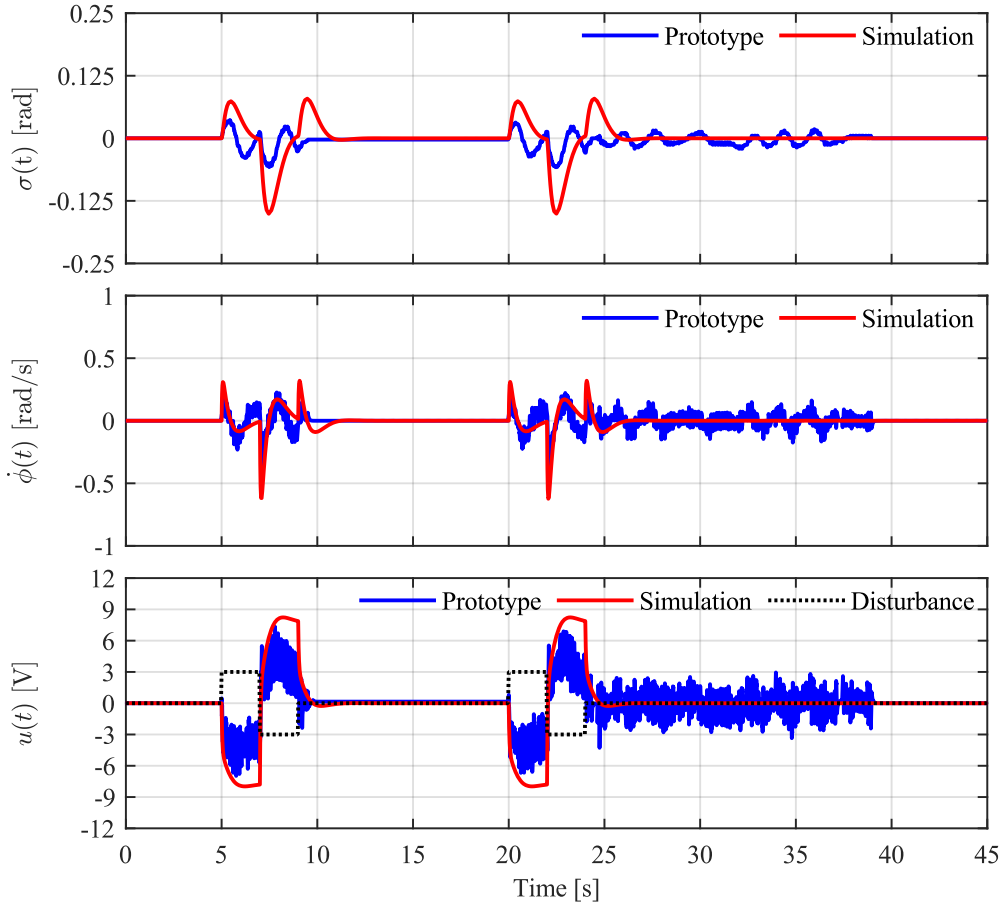


Figure 6. Results of simulation and of implementation on the RWIP prototype in the configuration M_{c1}, M_{r2} and I_{r2}.
Source: Authors, (2026).

Acknowledgments

The authors thank IFPR/Jacarezinho, UEM, the GAJAC laboratory (Garagem de Jacarezinho), and the Laboratory of Industrial Automation and Control (LAIC) for supporting the development of this work. The authors also thank IFPR and CNPq (grant numbers 190401/2025–7 and 190641/2025–8) for support in carrying out the work.

REFERENCES

[1] O. Boubaker, "The inverted pendulum benchmark in nonlinear control theory: A survey", International Journal of Advanced Robotic Systems, vol. 10, no. 5, (2013), pp. 233.

[2] R. Breganon, U. N. L. T. Alves, F. S. F. Ribeiro, G. V. Barbara, J. P. L. S. Almeida, L. E. Pivovar, M. A. F. Montezuma, and M. Mendonça, "Development of Inverted Pendulum Systems as Didactical Tools in Courses of Control and Automation Engineering", HOLOS, vol. 37, no. 5, (2021), pp. 1-13.

[3] T. Nazaré, J. P. Santos, I. Queinnec, and E. Nepomuceno, "A floating inverted pendulum model for analysing the pitch stability of offshore wind turbines", Nonlinear Science, vol. 5, (2025), pp. 100075.

[4] F. Asano, "Strict stealth walking of legged robot formed by four parallelogram links and equipped with wobbling mass and reaction wheel", IFAC-PapersOnLine, vol. 56, (2023), pp. 246-251.

[5] B. Lin, S. Zhang, S. Živanović, Q. Zhang, and F. Fan, “Verification of damped bipedal inverted pendulum model against kinematic and kinetic data of human walking on rigid-level ground”, Mechanical Systems and Signal Processing, vol. 200, (2023), pp. 1-20.

[6] A. Kharola, P. Patil, S. Raiwani, and D. Rajput, “A comparison study for control and stabilisation of inverted pendulum on inclined surface (IPIS) using PID and fuzzy controllers”, Perspectives in Science, vol. 8, (2016), pp. 187-190.

[7] A. N. K. Nasir, M. A. Ahmad, and M. F. Rahmat, “Performance comparison between LQR and PID controllers for an inverted pendulum system”, AIP Conference Proceedings, vol. 1052, (2008), pp. 124-128.

[8] F. H. Varaschim, F. A. Faria, M. C. M. Teixeira, A. L. S. Moscato, R. Breganon, and U. N. L. T. Alves, “Controle robusto H2 discreto via LMIs de um robô pêndulo invertido sobre duas rodas”, Simpósio de Engenharia de Controle e Automação, vol. 5, no. 1, (2024), pp. 1-10.

[9] U. N. L. T. Alves, R. Breganon, L. E. Pivovar, J. P. L. S. Almeida, G. V. Barbara, M. Mendonça, and R. H. C. Palácios, “Discrete-time H∞ integral control via LMIs applied to a Furuta pendulum”, Journal of Control, Automation and Electrical Systems, vol. 33, (2022), pp. 1-12.

[10] M. Castroviejo-Fernandez and I. Kolmanovsky, “Constrained reaction wheel desaturation and attitude control of spacecraft with four reaction wheels”, IFAC-PapersOnLine, vol. 56, (2023), pp. 6005-6011.

[11] S. Boyd, L. El Ghaoui, E. Feron, and V. Balakrishnan, Linear Matrix Inequalities in System and Control Theory. Philadelphia, PA, USA: Society for Industrial and Applied Mathematics, (1994).

[12] L. F. Buzachero, E. Assunção, M. C. M. Teixeira, and E. R. P. da Silva, “New techniques for optimizing the norm of robust controllers of polytopic uncertain linear systems”, Frontiers in Advanced Control Systems, (2012), pp. 75-100.

[13] M. L. M. Prado, “Controle robusto por alocação de pólos via análise intervalar modal”, Ph.D. thesis, Universidade Estadual de Campinas, Faculdade de Engenharia Elétrica e de Computação, Campinas, Brazil, (2006).

[14] H. F. Yamanaka, R. Breganon, F. A. Faria, R. Cardim, U. N. L. T. Alves, and M. C. M. Teixeira, “Controle integral robusto chaveado via LMIs de um sistema Aeropêndulo com incertezas paramétricas”, Revista Mundi Engenharia, Tecnologia e Gestão, vol. 9, no. 1, (2024), pp. 1-17.

[15] J. B. Santos, L. D. Silva, R. H. S. Souza, F. S. F. Ribeiro, R. Breganon, and U. N. L. T. Alves, “Controle via LMIs de um protótipo de pêndulo invertido com roda de reação”, Revista Mundi Engenharia, Tecnologia e Gestão, vol. 11, no. 2, (2026), pp. 1-14.

[16] R. H. S. Souza, J. B. Santos, L. D. Silva, R. Breganon, and U. N. L. T. Alves, “State-feedback control of a reaction-wheel inverted pendulum prototype”, Frontiers in Control Engineering, vol. 7, (2026), pp. 1905949.

[17] R. M. Silva, J. M. S. Ribeiro, R. Cardim, and M. C. M. Teixeira, “Classical and sliding mode controllers applied to the reaction wheel inverted pendulum”, IEEE Access, vol. 14, (2026), pp. 28884-28897.

[18] J. F. Sturm, “Using SeDuMi 1.02, a Matlab toolbox for optimization over symmetric cones”, Optimization Methods and Software, vol. 11, no. 1-4, (1999), pp. 625-653.

[19] J. Löfberg, “YALMIP: A toolbox for modeling and optimization in MATLAB”, IEEE International Symposium on Computer Aided Control Systems Design (CACSD), Taipei, Taiwan, (2004), pp. 284-289.

[20] K. Ogata, Engenharia de Controle Moderno, 5th ed. São Paulo, Brazil: Pearson, (2010).